

MODELLING THE MECHANICAL BEHAVIOUR OF THIN CMC COMPONENTS

C. Dupin^{1*}, G. Couégnat¹, E. Martin¹

¹Laboratoire des Composites ThermoStructuraux (LCTS), Univ. de Bordeaux; CNRS; SAFRAN-SPS;
CEA, 3 allée de la Boétie 33600 Pessac France

*dupin@lcts.u-bordeaux1.fr

Keywords: multiscale modelling, homogenization method, woven CMC, four-point bending tests.

Abstract

The aim of the paper is to develop an efficient homogenization technique to predict the effective mechanical properties of thin CMC materials that could be easily incorporated into a finite element framework for structural simulation of large CMC parts. The key idea of the proposed method is to perform an appropriate partition of the material microstructure into regular zones where the loading gradient could be considered as uniform. The properties of each zone are retrieved by performing a local homogenization of the underlying microstructure. This technique should allow capturing the effect of the varying material properties and its interaction with the macroscopic load gradient without the need to incorporate all the microstructural details.

1 Introduction

The next generation of commercial aircraft engine developed by Safran will incorporate several material innovations that would contribute to reduce their fuel consumption, pollutant emission and noise. Among these innovations, the use of Ceramic Matrix Composites (CMC) parts (e.g. compressor blade, exhaust system, etc.) will significantly contribute to reduce the overall mass of the engine. These CMC parts have a small thickness (<5mm) when compared to their structural size (from 10cm to 1m) that may vary over the part length. These variations may be due to local modification of the textile perform (weaving pattern, yarn density, weft/warp ratio, etc.) or to the manufacturing process (matrix deposition). Moreover, CMC materials exhibit an intricate and multiscale heterogeneous microstructure and their properties are strongly influenced by the size, shape and spatial distribution of their constituents (fibres, yarns, matrix, porosity). Therefore, the determination of the effective mechanical properties at every point of such CMC part is a challenging task since both the underlying material microstructure and the local macroscopic thickness influences them. A complete numerical simulation of CMC parts including all microstructural details would require too much computation resource to be considered as a feasible solution.

The aim of this paper is to propose a dedicated approach to design such thin CMC components. First the results obtained from an experimental campaign are presented. For this purpose, tensile and four-point bending tests have been performed on samples with different thicknesses. Then a finite element procedure based on a multiscale method which allows to select an optimal discretization of the CMC structure is proposed.

2 Experimental procedure

2.1. Material

The material used in the experimental studies is a SiC fibre reinforced SiC matrix composite, elaborated by Safran – Snecma Propulsion Solide. A woven fibre architecture with an interlock weaving is used (Figure 1). A pyrocarbon interphase and a self healing matrix have been deposited by chemical vapour infiltration. As reported in Table 1, four batches with a thickness ranging from 1.9 and 3.6mm have been characterized in tension and bending.

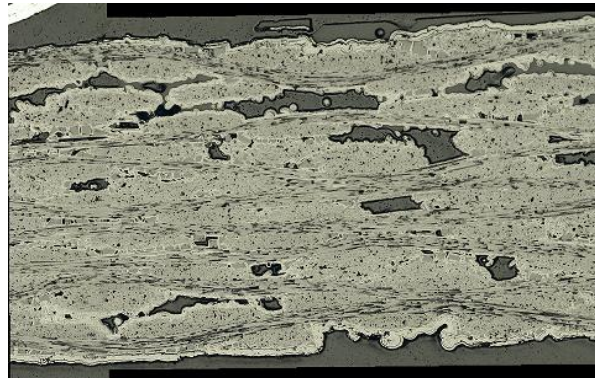


Figure 1. Cross-sectional optical micrograph of the SiC/SiC composite.

2.2. Tensile tests

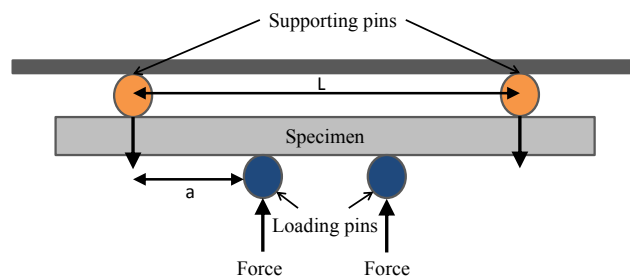
Tensile tests are used to identify the in-plane elastic properties of the materials. The tests are carried out with a 50kN frame (servohydraulic Instron 4505) under a displacement control (0.05mm/min). The specimens are cut out from a composite plate in the 0° direction with respect to the weave pattern. Two extensometers with a gage length of 10mm are used for the strain measurements in the load direction. Aluminum tabs are glued on each end of the specimens to avoid damaging the material from tightening in the hydraulic grip

2.3. Four points bending tests

Four points bending tests are carried out with the help of the testing device schematically shown in Figure 2b. The used assembly includes two supporting pins, two loading pins and a deflection transducer (Figure 2a). The originality of this device resides in the trim control system, which allows to keep loading pins perfectly horizontal.



(a)



(b)

Figure 2. (a) Four points bending feature with $L=80\text{mm}$ and $a=25\text{mm}$, (b) schematic view of the bending parameters.

The loading speed is 0.05mm/min. The dimension of the specimen is 120mm long and 15mm wide. In the case of a homogeneous beam, without taking into account the transversal shear, the flexural modulus E_{flex}^1 is given by [1]:

$$E_{flex}^1 = \frac{\Delta P}{\Delta f(0)} \frac{(3aL^2 - 4a^3)}{4bh^3} \quad (1)$$

where b is the width, h is the thickness, ΔP is the loading force, $\Delta f(0)$ is the deflection measurement, L is the distance between supporting pins and a is the distance between supporting pins and loading pins (Figure 2b).

The calculation of deflection taking into account the transversal shear is given by :

$$\Delta f = \Delta f(0) \left(1 + \frac{2h^2 E_{flex}}{(3L^2 - 4a^2)G_{xz}} \right) \quad (2)$$

where G_{xz} is the shear modulus.

This last expression shows that it is possible to determine E_{flex}^2 from the measurement of the slope $\frac{\Delta f}{\Delta P}$, obtained for two couples (L_1, a_1) and (L_2, a_2) with :

$$E_{flex}^2 = \frac{3(L_1^2 - L_2^2) - 4(a_1^2 - a_2^2)}{4bh^3 \left(\frac{\Delta f_1}{\Delta P_1} \frac{1}{a_1} - \frac{\Delta f_2}{\Delta P_2} \frac{1}{a_2} \right)} \quad (3)$$

2.4. Results

Figure 3a depicts the mechanical response in terms of strain-force for the tensile tests (Figure 3a) and deflection-force for the bending test (Figure 3b). Recording of acoustic emission is also plotted to detect the activation of cracking mechanisms.

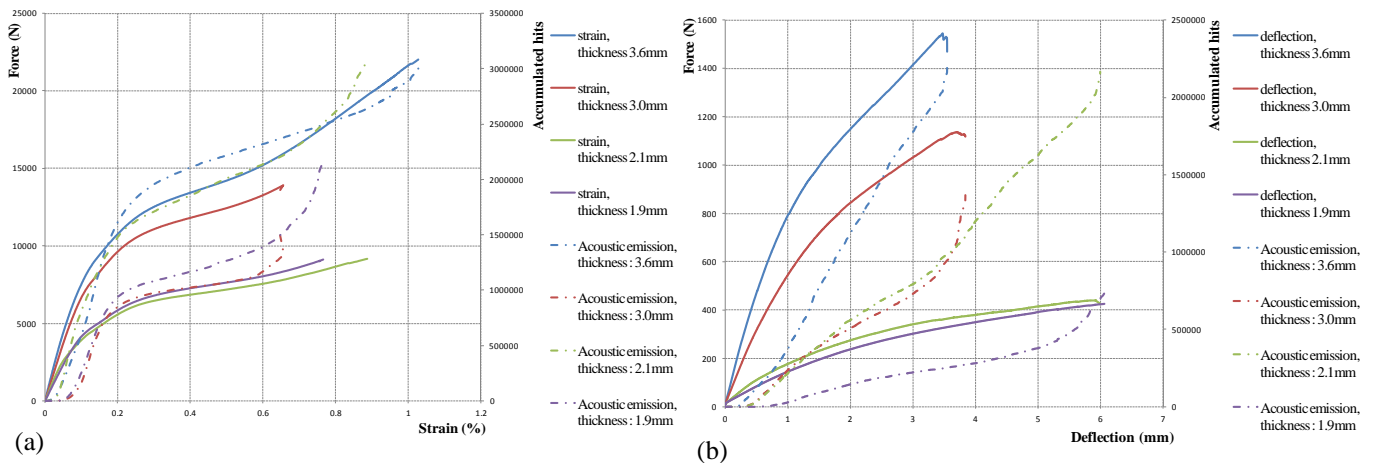


Figure 3. Influence of the thickness : (a) on the tensile response, (b) on the four points bending response for $L_1=80mm$ and $a_1=25mm$.

Both traction and flexion results exhibit the typical behaviour of a SiC/SiC composite : a linear part (without acoustic emission) followed by a damaging phase, corresponding to the development of crack networks until the fracture of the material.

Four other bending test were carried out with the configuration $L_2 = 55mm$ and $a_2 = 15mm$.

Table 1 reports the longitudinal Young modulus E_{trac} , determined by the tensile test, the flexural modulus as evaluated with (1) and (3) :

| <i>Properties</i> | <i>material A</i> 3.6 mm | <i>material B</i> 3.0 mm | <i>material C</i> 2.1 mm | <i>material D</i> 1.9 mm |
|--------------------|-----------------------------|-----------------------------|-----------------------------|-----------------------------|
| E_{trac} (GPa) | 162 | 160 | 167 | 153 |
| E_{flex}^1 (GPa) | 120 | 147 | 140 | 132 |
| <i>error</i> | 26 % | 8.1 % | 16.2 % | 13.7 % |
| E_{flex}^2 (GPa) | 141 | 153 | 160 | 135 |
| <i>error</i> | 13 % | 4.3 % | 4.1 % | 11.8 % |

Table 1. Comparison between Young modulus identified by a tensile test and by a four points bending test (with and without taking into account the transversal shear) for different thicknesses.

Table 1 makes clear that flexural modulus may be significantly lower than the tensile modulus depending on the thickness and thus on the microstructure. The next section thus describes a multiscale approach which attempts to explain this discrepancy.

3 Modelling procedure

3.1. Generation of woven composites and determination of effective properties

The first step is the building of a cell which represents at best the various peculiarities of the microstructure (porosity, architecture, gradient of infiltration, manufacturing, etc.). Previously developed tools [2] allow to generate a geometrical model of the weaved reinforcement and to create 2D finite elements meshing of the weaved reinforcement (Figure 4a) which are “numerically” infiltrated by the matrix.

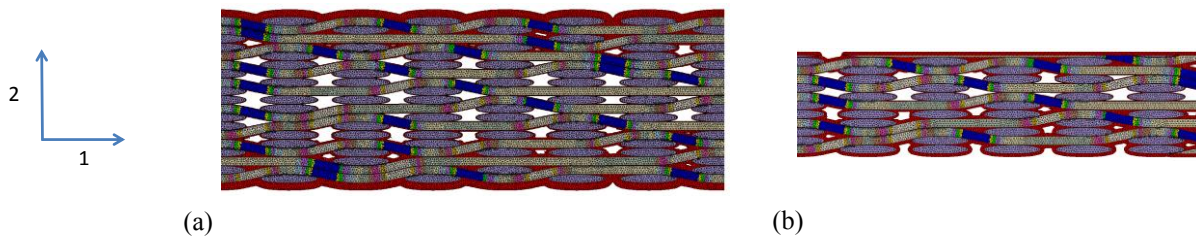


Figure 4. (a) 2D meshing cell with gradient of infiltration, (b) 2D manufactured and re-densified meshing cell.

This procedure provides various cells representative of texture, gradients of infiltration as well as manufacturing cycles with re-densification.

Then, detailed numerical calculations are performed using these representative cells. Both tension and bending loading are considered to determine the effective properties of the material. Non-homogeneous boundary conditions [3] are used :

$$u_i = E_{ij}x_j + \delta_{ijk}K_{jl}x_lx_k, \quad \text{for each point of the domain frontier} \quad (4)$$

where tensor E (respectively K) has the meaning of an imposed strain (respectively a prescribed curvature). The third-rank permutation tensor is denoted δ . If K vanishes, classical

boundary conditions, representative of tensile and shear loading, are retrieved. If only K_{31} is non-zero, we get :

$$\begin{cases} u_1 = -K_{31}x_1x_2 \\ u_2 = K_{31}x_1^2 \end{cases} \quad (5)$$

which imposes a flexural loading. Figure 5 summarizes the determination of the relevant effective properties in the two-dimensional case.

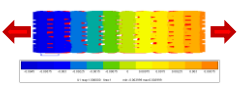
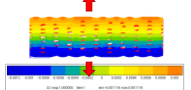
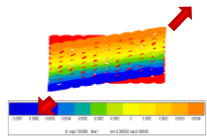
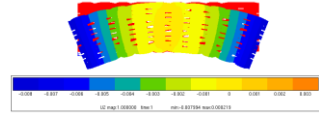
| Tensile test | | | Flexion test |
|--|--|--|--|
| $\begin{cases} E_{11} = 1 \\ E_{33} = 0 \end{cases}$ et $\begin{cases} E_{13} = 0 \\ K_{31} = 0 \end{cases}$ | $\begin{cases} E_{11} = 0 \\ E_{33} = 1 \end{cases}$ et $\begin{cases} E_{13} = 0 \\ K_{31} = 0 \end{cases}$ | $\begin{cases} E_{11} = 0 \\ E_{33} = 0 \end{cases}$ et $\begin{cases} E_{13} = 1 \\ K_{31} = 0 \end{cases}$ | $\begin{cases} E_{11} = 0 \\ E_{33} = 0 \end{cases}$ et $\begin{cases} E_{13} = 0 \\ K_{31} = 1 \end{cases}$ |
|  |  |  |  |
| $\begin{cases} C_{11} = \frac{1}{V} \int_{\Omega} \sigma_{11} d\Omega \\ C_{13} = \frac{1}{V} \int_{\Omega} \sigma_{22} d\Omega \\ C_{15} = \frac{1}{V} \int_{\Omega} \sigma_{12} d\Omega \end{cases}$ | $\begin{cases} C_{31} = \frac{1}{V} \int_{\Omega} \sigma_{11} d\Omega \\ C_{33} = \frac{1}{V} \int_{\Omega} \sigma_{22} d\Omega \\ C_{35} = \frac{1}{V} \int_{\Omega} \sigma_{12} d\Omega \end{cases}$ | $\begin{cases} C_{51} = \frac{1}{V} \int_{\Omega} \sigma_{11} d\Omega \\ C_{53} = \frac{1}{V} \int_{\Omega} \sigma_{22} d\Omega \\ C_{55} = \frac{1}{V} \int_{\Omega} \sigma_{12} d\Omega \end{cases}$ | $M_{31} = \frac{1}{V} \int_{\Omega} (\sigma_{11}y_{\Omega} - \sigma_{12}x_{\Omega}) d\Omega$ |

Figure 5. Determination of effective properties.

3.2. Classical first order homogenization scheme

The physical and geometrical properties of the microstructure are identified by a representative volume element (RVE). In the ideal case, the RVE should be chosen to be statistically representative of the microstructure of the material. The choice of the size of the RVE is conditioned by three parameters:

- d : characteristic size of heterogeneities,
- L : size of the discrete elements used in the global model
- l : length of the RVE

The ratio l/d has to be large enough to allow a significant sampling of the microscopic fields. It is also necessary that the structure can be treated as a continuous environment. This condition is classically denoted in the following way:

$$d \ll l \ll L \quad (6)$$

For example, let us consider a very simple cell constituted by a weft yarn, by two warp yarns, densified by the matrix (Figure 6a). Its effective properties are calculated (C_{ij}^{micro} and M_{31}^{micro}), then a homogeneous equivalent beam is considered (Figure 6b) on which the flexural rigidity $M_{31}^{homogene}$ is calculated.



Figure 6. (a) RVE meshing cell, (b) homogeneous equivalent model.

Then, new cells representing several times the RVE are generated (Figure 7a). Flexural rigidity M_{31}^{micro} is calculated and compared with $M_{31}^{homogene}$ in Figure 7b.

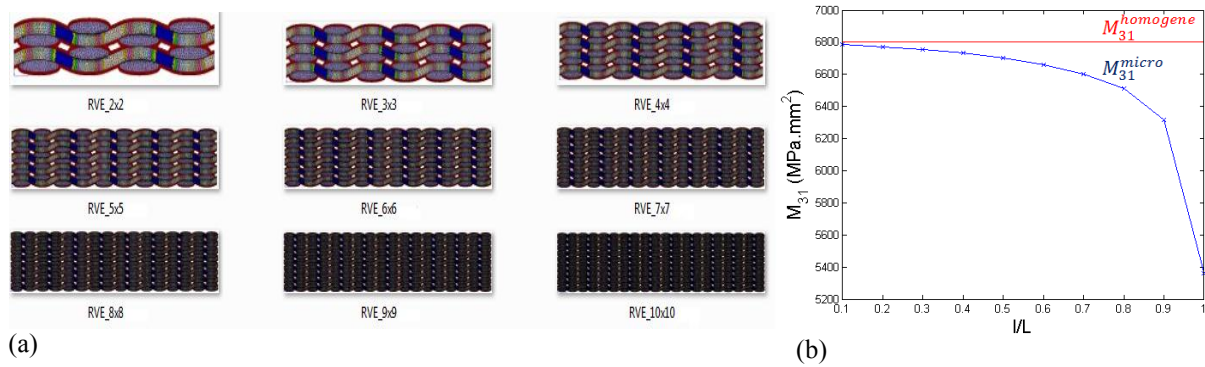


Figure 7. (a) cells containing several RVE, (b) flexural rigidity M_{31} versus the ratio l/L .

This plot confirms that if a RVE is clearly defined and equation (6) is satisfied, then classical homogenization works relatively well. Nevertheless, this classical first-order homogenization scheme [4] proved to be inappropriate for our applications since (i) the considered materials do not clearly exhibit a representative volume element, and (ii) for mechanical loading involving an out-of-plane component (e.g. bending, torsion), the characteristic wave length of the macroscopic loading is of the same order than the characteristic size of the material [5]. The aim of the next part is to develop an efficient homogenization technique to predict the effective mechanical properties of thin CMC materials that could be easily incorporated into a finite element framework for structural simulation of large CMC parts.

3.3. Partition of the properties field

The key idea of the proposed method is to perform an appropriate partition of the material microstructure into regular zones where the loading gradient could be considered as uniform and where the properties of each zone are retrieved by performing a local homogenization of the underlying microstructure (Figure 8). For all calculations at the microstructure scale, the matrix SiC is considered to be isotropic with a Young modulus equal to 400GPa and Poisson coefficient equal to 0.2. Both warp and weft yarns are considered as orthotropic materials. The relevant elastic properties are evaluated with the help of a homogenization procedure performed on a cell representative of a yarn (the longitudinal modulus is 250 GPa).

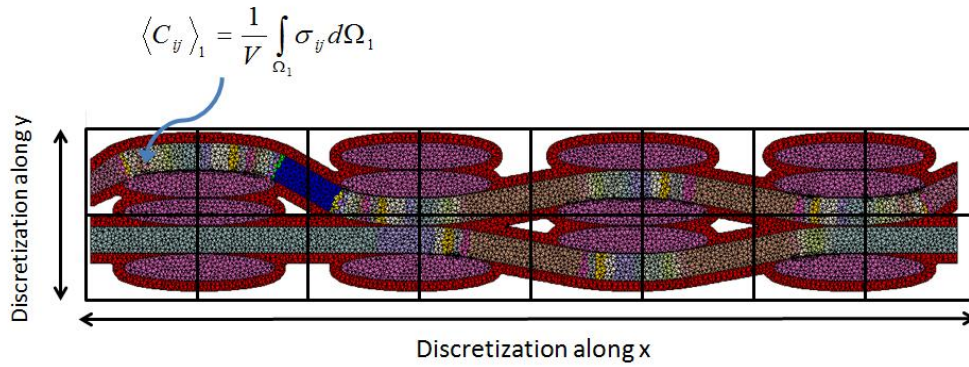


Figure 8. Partition of the homogenization field.

The partition is iteratively refined (Figure 9a) until the effective flexural rigidity computed using the mosaic approximation M_{31}^{mosaic} is close enough to the one estimated from the full microstructural calculation (Figure 9b).

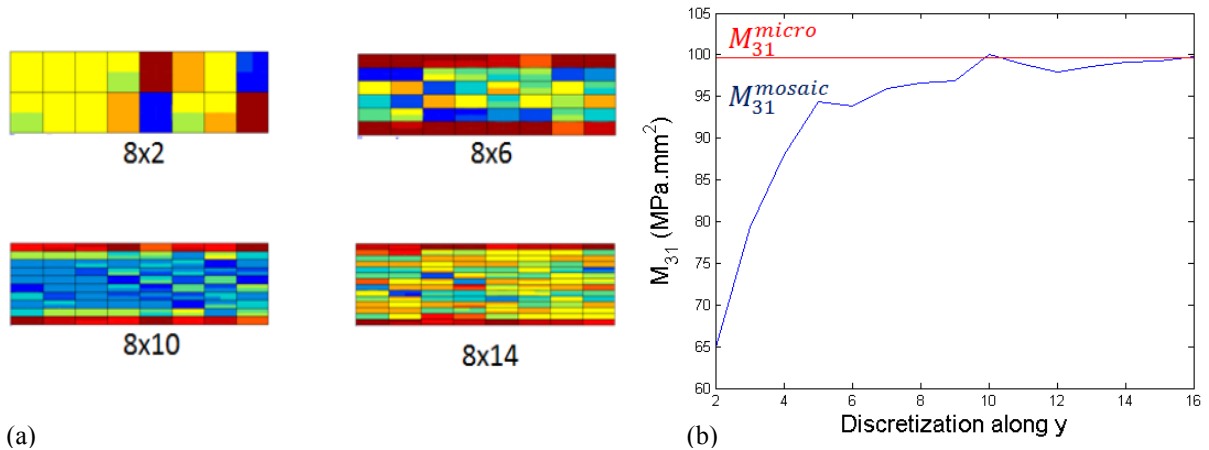


Figure 9. (a) few examples of distributions of mechanical properties, (b) Comparison between the calculation of the flexural rigidity obtained by the mosaic model and the full microstructural model according to the spatial discretization.

Calculations were led for various textures and types of infiltration. For all the cells studied, flexural rigidity using equivalent homogeneous model is between 10 and 35% lower than flexural rigidity using the full microstructural model. It is worthy of note that a similar tendency is observed from experimental results (Table 1). The mosaic model reproduces well the behaviour of the microstructure in terms of in-plane elastic rigidity (C_{ij}) and flexural rigidity.

4. Conclusion

A finite element procedure based on a multiscale method which allows to select an optimal discretization of the CMC structure is proposed. Instead of considering only the effective mechanical behaviour as calculated by a conventional homogenization approach, an appropriate partition of the material microstructure into regular zones where the properties of each zone are retrieved by performing a local homogenization of the underlying microstructure is performed. A 3D reference model is scheduled based on the voxel element method. Further work will focus on the adaptation of this homogenization technique to 3D cells with variations in thickness.

Experimental results seem to corroborate numerical calculations. Short beam bending tests will be performed and compared with numerical finite element simulation using the proposed homogenization technique.

References

- [1] Berthelot J.-M. *Matériaux composites : Comportement et analyse des structures*. Masson, Paris (1992).
- [2] Couegnat G., Martin E., Lamon J. *Multiscale modelling of the mechanical behaviour of woven composite materials* in "Proceeding of International Committee on Composite Materials – 17", Edinburgh, United Kingdom, (2009).
- [3] Forest S. Mechanics of generalized continua : construction by homogenization. *J. Phys. IV*, **4**, pp. 39-48 (1998).
- [4] Bornert M., Bretheau T., Gilormini P. *Homogénéisation en mécanique des matériaux 1 : matériaux aléatoires élastiques et milieu périodiques*. Hermès, Paris (2001).
- [5] Geers M. G. D., Kouznetsova V., Brekelmans W. A. M. Gradient-enhanced computational homogenization for the micro-macro scale transition. *J. Phys. IV*, **11**, pp. 145-152 (2001).